Proceedings World Geothermal Congress 2020+1
Reykjavik, Iceland, April - October 2021

Assessment of the Ability of GIS Based MCDA Methods to Reveal the Geothermal Potential of the Büyük Menderes Graben

Gozde P. Yal[1], Selim Cambazoglu[1], A. Mert Eker[2], Osman Sen[2], Haluk Akgun[1]

[1] Geotechnology Unit, Department of Geological Engineering, Middle East Technical University, Ankara, Turkey

2 SDS Enerji A.S., Ankara, Turkey

gozdeyal@gmail.com

Keywords: GIS, MCDA, Western Anatolia, geothermal favorability, Büyük Menderes Graben.

ABSTRACT

More than 80% of the geothermal electricity production of Turkey is currently attained by the Büyük Menderes Graben, with further potential yet to be revealed. The majority of the early development has been on the main plain of the graben; however, in recent years new sites with great geothermal potential have been discovered at the northern flank of the graben. The geothermal system in Western Anatolia is governed by a N-S extensional regime represented by high angle E-W trending normal faults. The heat transfer achieved through a fault controlled convective system led to the formation of many low-to-high enthalpy geothermal areas at the northern flank of the graben. The general success rate of geothermal drilling tends to decrease away from the graben center. Thus, every means that could guide the search for new geothermal sites should be made available prior to drilling exploratory wells, which account for the majority of the cost in geothermal exploration studies. The GIS based multi-criteria decision analysis (MCDA) serves as an invaluable tool in an attempt to minimize the risks of geothermal exploration by revealing areas with high potential as an initial assessment. In this study, a knowledge-based MCDA method has been employed in order to determine the geothermal potential map of the Büyük Menderes Graben. Criteria including geological, seismo-tectonic, topographic, surface temperature and vegetation data have been used for the spatial assessment of the geothermal potential of the Büyük Menderes Graben. The ability of MCDA to reveal the true geothermal potential of the area was evaluated by comparing the generated favorability map with the known locations of producing geothermal wells. As a result, 95% of the producing wells corresponded to the classes identified as most favorable (76%) and favorable (19%).

1. INTRODUCTION

Turkey is ranked 4th in the world in terms of current installed geothermal capacity, and acts as one of the leaders in geothermal development, with an exponential growth over the last decade (Richter, 2018). The total installed capacity was below 200 MWe in year 2012, which increased to 1347 MWe as of year 2018. With the sites under construction and development, the capacity is expected to exceed 2000 MWe by 2020.

The early development started mainly at the licenses located close to the graben center, followed by development towards the northern flank of the graben due to the lack of unoccupied licenses close to the center. While the search of new geothermal resources led to the discovery of many new geothermal sites with good potential, considerable amount of money had been invested to sites that lack any feasible resources.

In this study, in an attempt to reduce the risks of geothermal development, a geothermal favorability map of the Büyük Menderes Graben has been generated by employing several decision criteria (explanatory variables) layers, including distance to faults, fault density, distance to hot springs, distance to cap rocks, distance to the graben center, night time surface temperature, b-value, slope angle and normalized difference vegetation index (NDVI). Each layer was introduced into a GIS environment where a multi-criteria decision analysis (MCDA) method was employed to generate a geothermal favorability map divided into 6 favorability classes. The success of the methodology was assessed by comparing locations of the known producing wells with the resultant map.

2. STUDY AREA AND GEOLOGICAL SETTING

The study is located in the Büyük Menderes Graben, which is located at the Aegean Region in western Turkey. The region mainly covers the Aydin Province and part of Denizli and Izmir Provinces, and has an area of approximately 12,000 km^2 (Figure 1). The Büyük Menderes Graben system trends in the E-W direction at the central and eastern section and in the NE-SW direction at the western section along with small scale horst-graben structures trending perpendicular to this main horst-graben structure.

Western Anatolia is represented by a high-rate continental crust seismic activity and extension. The current setting of the region is N-S continental extensional regime (Bozkurt and Sözbilir, 2006) with 3-4 cm annual extension rate (Ferill et al., 1996; Kahle et al., 2000). This extension is compensated by slip on the active normal faults with high seismicity (Eyidoğan and Jackson, 1985).

The tectonic framework in the region presents a complex structure. Causes and initiation of continental extension is an ongoing debate in the literature where different models have been proposed over the years (Bozkurt and Sözbilir, 2006). These include the Tectonic Escape Model (Şengör et al., 1985; Görür et al., 1995), Back-Arc Extension Model (McKenzie, 1978), Orogenic Collapse Model (Seyitoğlu et al., 1991) and Episodic Model (Koçyiğit et al., 1999).

Paleozoic age Menderes Massif metamorphic units are located at the bottom of the stratigraphic succession in the region. Menderes Massif Metamorphic units, the oldest formations in the region, act as the basement rock of the study area. Menderes Massif is a regional, large scale, NE-SW trending metamorphic core complex (Verge, 1995; Bozkurt and Park, 1997; Bozkurt, 2001 and Koçyiğit, 2015). These units are composed of metamorphic rocks with irregular lithological characteristics in horizontal and

vertical directions, including marble, various schist, quartzite and gneiss units. The marble layers in the Menderes Metamorphics act as the reservoir rock of the system, overlain by the Miocene and Pliocene age Neocene deposits. Quaternary deposits, presenting a significant distribution throughout Menderes Graben, are located at the top of the succession over the Neocene deposits. The fine grained sedimentary sequence of the graben fills have low permeability, allowing them to serve as the cap rock of the geothermal system along with the schistic levels of the Menderes Massive and Neocene deposits at places (Figure 2).

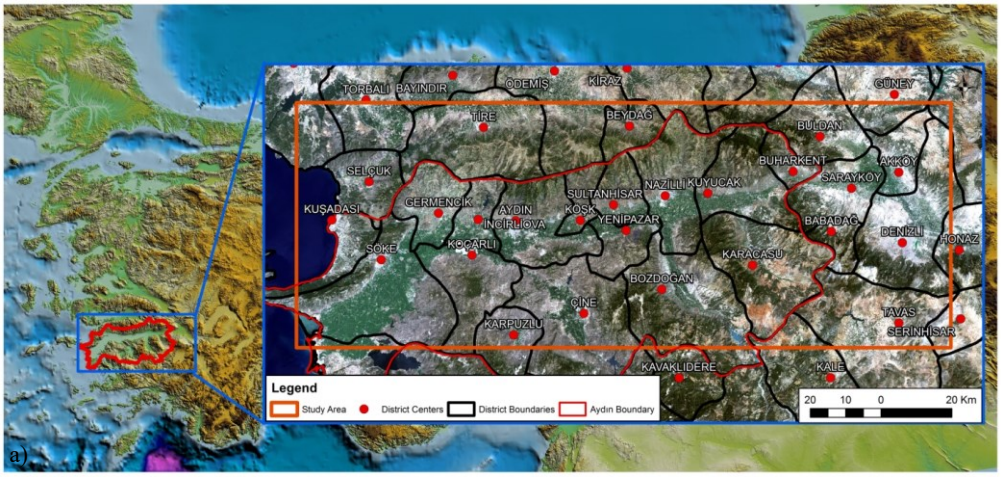


Figure 1. Study area showing the Aydin Provincial boundaries overlain on shaded relief map, and a true color composite of 20.07.2015 LandSat 8 satellite image.

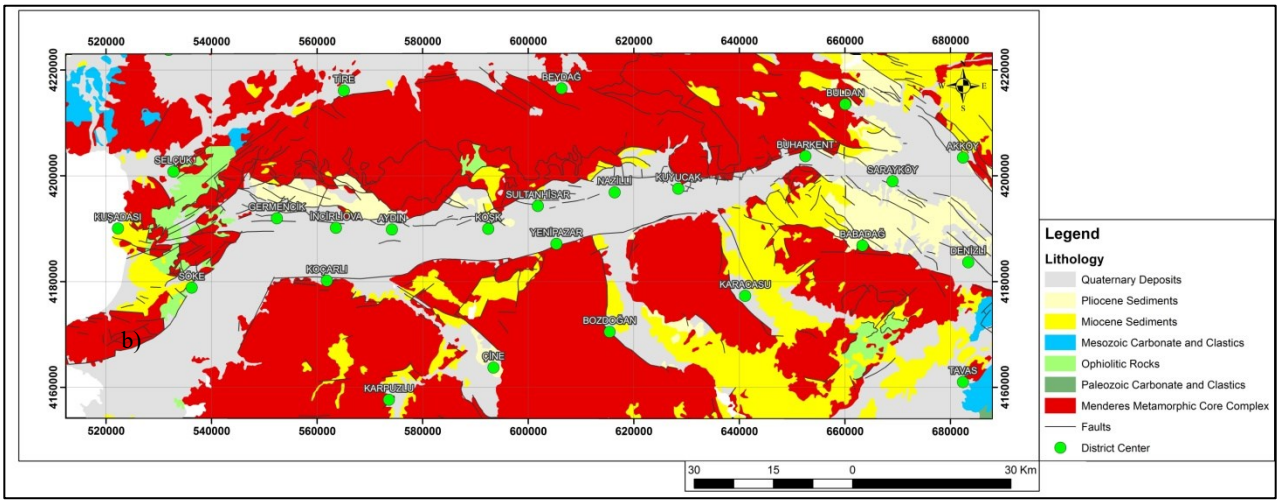


Figure 2. Generalized geological map of the study area.

3. METHODOLOGY

In this study, a knowledge driven method has been employed where the relative importance of each criterion is determined by the judgment of the expert. Index overlay (Prol-Ledesma, 2000; Noorollahi et al., 2008), weighted linear combination (Noorollahi et al., 2007; Yalcın and Gul, 2017; Kiavarz and Jelokhani-Niaraki, 2017), fuzzy scheme models (Prol-Ledesma, 2000), Technique for Order Preference by Similarity to the Ideal Solution (TOPSIS) (Cambazoğlu et al., 2019) and Boolean logic (Yousefi et al., 2007; Noorollahi et al., 2008; Yousefi et al., 2010) are some examples of knowledge based methods. In the scope of this study, TOPSIS methodology has been followed to generate the favorability map of the Büyük Menderes Graben by using a number of datasets. Each dataset or attribute has the ability to distinguish a geographical entity. The datasets, the criteria maps generated from these datasets and their sources are tabulated in Table 1.

A multi-collinearity analysis was conducted where the tolerance and Variance Inflation Factor (VIF) values were obtained. Tolerance is the percent of the variance in a given predictor that cannot be explained by the other predictors (Norusis, 2004). Low tolerance values indicate that around 70-90% variance of an explanatory variable can be explained by other explanatory variables. When the tolerance is close to 0, there exists a high multi-collinearity and the standard error of the regression coefficients will be inflated. As a result of the multi co-linearity analysis, the obtained VIF values were below 5 and the tolerance values were above 0.2 m (Menard, 1995; Rogerson, 2001) demonstrating the lack of any major interdependency between these attributes.

A total of nine layers were used including distance to fault, fault density, distance to graben center, distance to cap rock, distance to hot spring, b-value, night-time surface temperature, slope angle and NDVI. Each standardized layer is ranked according to their relative importance and assigned a weight value by employing a pairwise comparison method (Malczewski, 1999). The Pairwise Comparison Method allows determining the relative importance of an entity by comparing all entities in pairs (Saaty, 1980).

Table 1. Dataset and their source

Dataset	Criteria maps	Source
Hot spring	Distance to hot springs	Akkuş et al., 2005
Fault map	Fault density Distance to fault	MTA, 2002; Gürer (2009); Duman et al. (2011); Koçyiğit (2015)
LANDSAT	Vegetation-NDVI	USGS-EROS, 2017
ASTER-TIR	Night-time surface temperature	NASA LP DAAC, 2017
DEM	Slope angle	General Command of Mapping, 2000
Geological map	Neocene cap rock	MTA, 2002
Regional geophysical data	Distance to graben center	Arslan et al., 2010; Çiftçi and Bozkurt, 2010
Earthquake epicenter	Gutenberg-Richter b-value	KOERI, 2019

In application of the TOPSIS methodology, initially the negative ideal and positive ideal points for each weighted standardized map were obtained by determining the minimum and maximum value of each attribute. The Euclidean distance between the negative and positive ideal layers and the weighted standardized maps were generated. Further, the relative closeness to the ideal point was determined by adding the Euclidean separations and by dividing the resultant map to the Euclidean distance to the positive ideal (Malczewski, 1999). Thus, the final favorability map of Büyük Menderes Graben was obtained.

The extent of the layers were bounded by the area covering the geothermal wells drilled in the area since the success of the final favorability map was assessed by comparing the final map with the successful drillings. Information on each attribute and the ranking procedure used to generate the criteria maps from the datasets are described below.

3. DATASETS AND RESULTS

A generalized fault map has been created by using the major faults in Büyük Menderes Graben as identified by MTA (2002), Gürer (2009), Duman et al. (2011), and Koçyiğit (2015). The distance to the fault layer was generated by using Euclidian distance to fault lines and the values of the resultant layer (30 m x 30 m resolution) ranged between 0 and 22.14 km with a mean value of 3.5 km (Figure 3).

In addition to the distance to the fault map, in order to emphasize the importance of highly fractured areas in an extensional regime, a fault density map has also been generated. In order to account for the importance of the low dipping crustal scale detachment fault (Gessner, 2013) displaced by the high angle normal faults, a weight factor of 2 has been used for the detachment fault. The fault density map was generated with a 4.6 km search radius. This radius was identified by considering the average earthquake epicenter depth falling within the study area (8 km) (KOERI, 2019) and fault dip angle of 60°, and generated with 30 m x 30 m resolution (Figure 4).

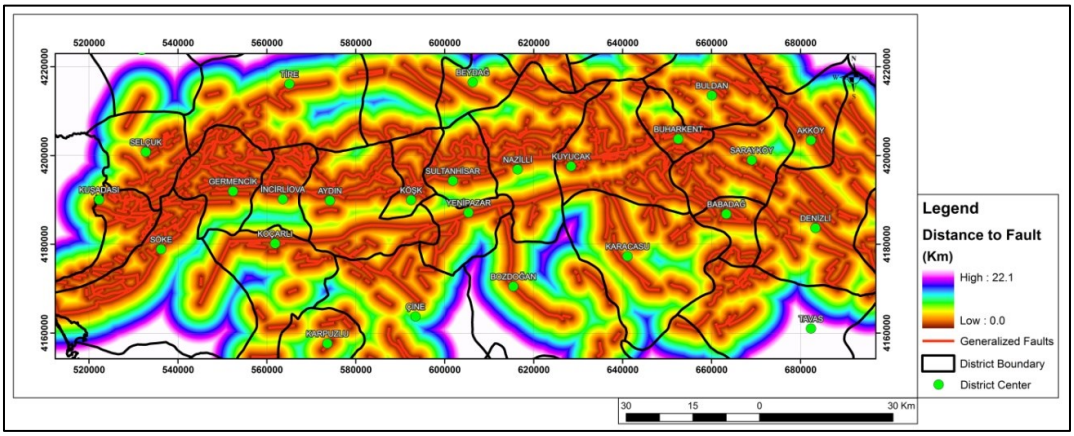


Figure 3. Distance to fault map of the study area.

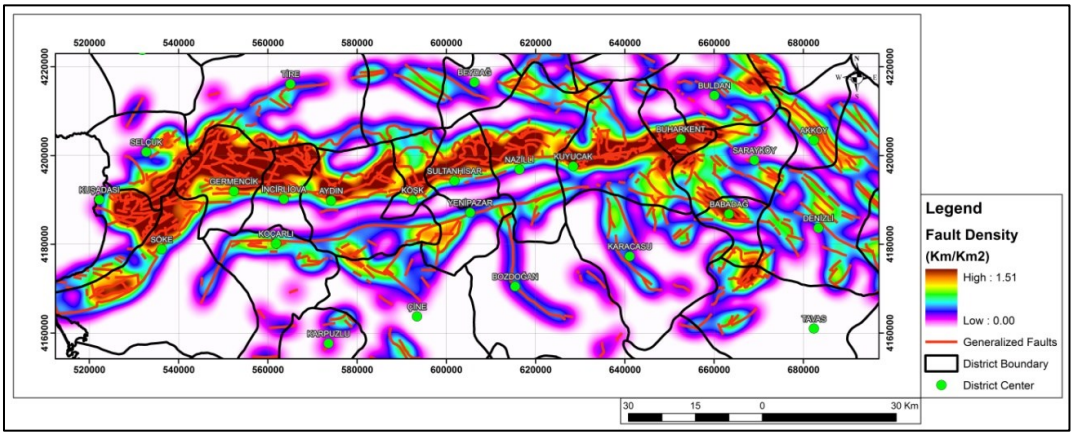


Figure 4. Fault density map of the study area.

Hot spring locations are one of the major surface manifestations of a geothermal system. Major hot spring locations were digitized from Akkuş et al. (2005) with several additions from field surveys. The distance to hot spring map was generated by using Euclidian distance with a resolution of 30 m (Figure 5).

The distance to the cap rock map was generated by using the 1:500000 scale geological map of the region (MTA, 2002). The cap rock of the geothermal system in the Büyük Menderes region is Neogene and Quaternary deposits that unconformably overly the pre-Neogene basement Menderes Massif units (Yılmazer et al., 2010). However, it should also be noted that there are geothermal fields with great potential located relatively far away from the graben center, where the schist levels of the Menderes Massive serve as the cap rock of the geothermal system compensating for the thinning of the Quaternary and Neogene cap rock layers (Yal et al., 2017). Thus, the cap rock was included as a distance map instead of a binary classifier and the digitized geological map was used to generate a distance to Neocene and Quaternary units layer with a resolution of 30 m (Figure 6).

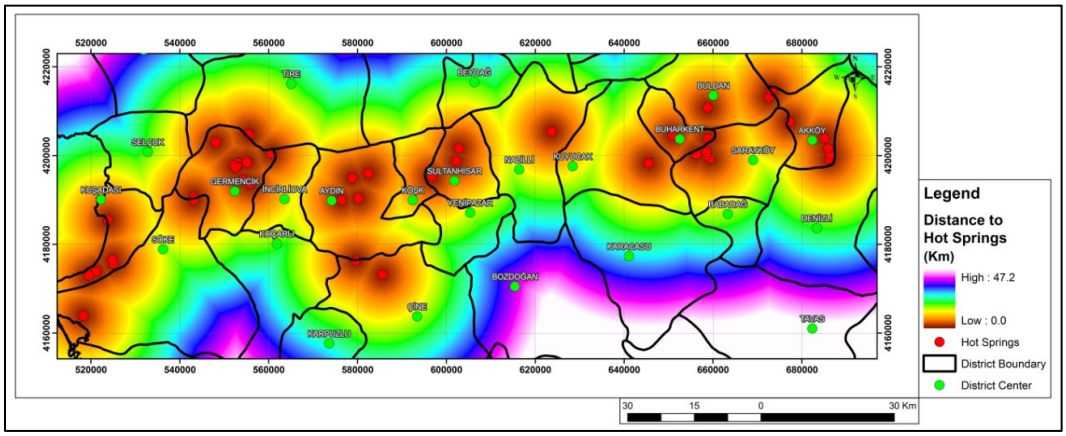


Figure 5. Distance to hot spring map of the study area

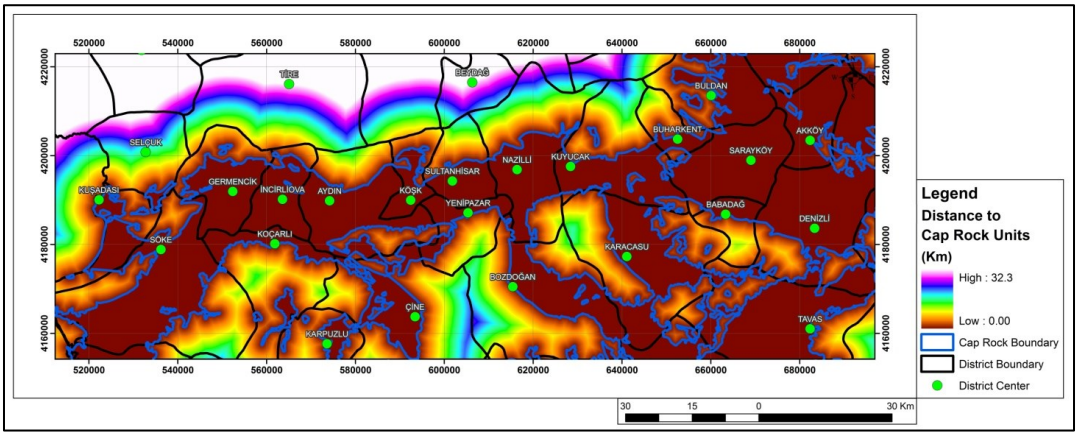


Figure 6. Distance to cap rock units (cap rock unit boundaries are shown as blue lines).

The graben center is identified by using 1:1250000 scale regional geophysical maps (free air gravity and Bouger gravity maps) (Arslan et al., 2010), and 1:500000 scale geological map (MTA, 2002). The major geothermal activity is located at the northern

section of the graben and this area is known to be more seismically active. Therefore, since the geothermal favorability decreases away from the graben center, to achieve a slower decay of favorability at the northern section, a Euclidian distance map was generated by using a weight factor of 0.5 for the northern section of the graben (Figure 7).

The night-time surface temperature was included as a criterion layer to detect any temperature anomaly as an indicator of a shallow heat source. The layer was generated by using ASTER L1T satellite image data (NASA LP DAAC, 2015), courtesy of the NASA Land Processes Distributed Active Archive Center (LP DAAC), USGS/Earth Resources Observation and Science (EROS) Center, Sioux Falls, South Dakota. In order to cover the entire study area, a total of 17 ASTER images were used. A surface temperature image was generated by applying emissivity and temperature separation algorithm (Hook et al., 1992; Gillespie et al., 1998) on the five thermal infrared (TIR) bands of ASTER with 90 m spatial resolution. ASTER images were mosaicked and elevation correction was applied on the mosaic image. An environmental lapse rate of -4.6°C/km was used which was estimated from the linear regression between night-time surface temperature and elevation data (Eneva and Coolbaugh, 2009; Gutierrez et al., 2012) (Figure 8).

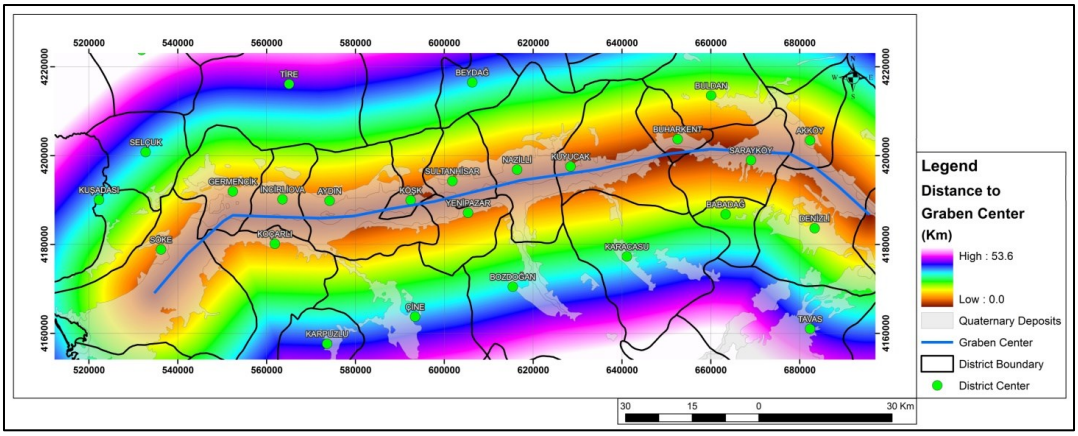


Figure 7. Distance to graben center map.

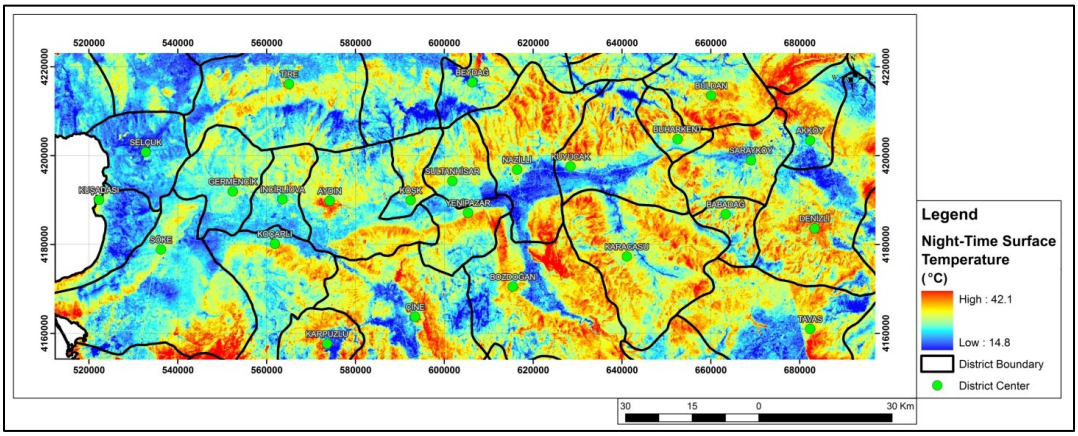


Figure 8. Night-time surface temperature map.

As a seismo-tectonic parameter, the Gutenberg-Richter (1949) b-value map was generated by Z-Map seismic analysis software package (Weimer, 2001). The b-value is a seismo-tectonic parameter directly related with the earthquake occurrence (Gutenberg and Richter, 1949). This value is calculated by log(N) = a - b(M) relation proposed by Gutenberg and Richter (1949), where N is the number of earthquakes with magnitude equal to or larger than M, and 'a' and 'b' are regression coefficients. The earthquake catalogue of Kandilli Observatory and Earthquake Research Institute encompassing the earthquake data between 1900 and 2019 was used (KOERI, 2019). Primarily de-clustering analyses based on time and spatial windows proposed by Gardner and Knopoff (1974) was performed on the earthquake database in order to ensure that the catalogue represents Poisson relation used to represent the earthquake phenomenon in time domain, and also to ensure mutual exclusiveness of the events. Following the exclusion of secondary events out of a total of 3922 events having Mw>3.0, the final de-clustered catalogue included 1488 earthquakes. The final b-value map was generated with a 30 km search radius and 500 m x 500 m resolution, resampled to 30m x 30 m (Figure 9).

Slope angle layer has been included as an indirect identifier of the geothermal potential since lack of feasible access to a region may hinder the development potential of that region. The slope angle layer map was generated from DEM created with a 30 m resolution by using digitized contours of the 1:25000 scale topographical maps. The slope values in the study area ranged between 0° and 57° with a mean value of 11.3° and a standard deviation of 9.5°. The resultant slope angle map was reclassified into four discrete classes as: 1 for values lower than 10°, 0.5 for values between 10° and 20°, 0.25 for values between 20° and 30°, and 0 for values higher than 30°, respectively (Figure 10).

A Normalized Difference Vegetation Index layer was generated by using Landsat 8 OLI&TIRS image acquired on July, 2013 (USGS-EROS, 2019). Near-Infrared (NIR) and Red bands of Landsat 8 image were used to calculate the NDVI layer. NDVI =

(NIR-RED)/(NIR+RED), which represents the vegetation density, varying between -1 to 1, where the higher values indicate healthy vegetation. Mean plus one standard deviation (0.39) is used to classify the NDVI layer as a binary variable (Figure 3a) where 0 was assigned to the values above 0.39 (Figure 11).

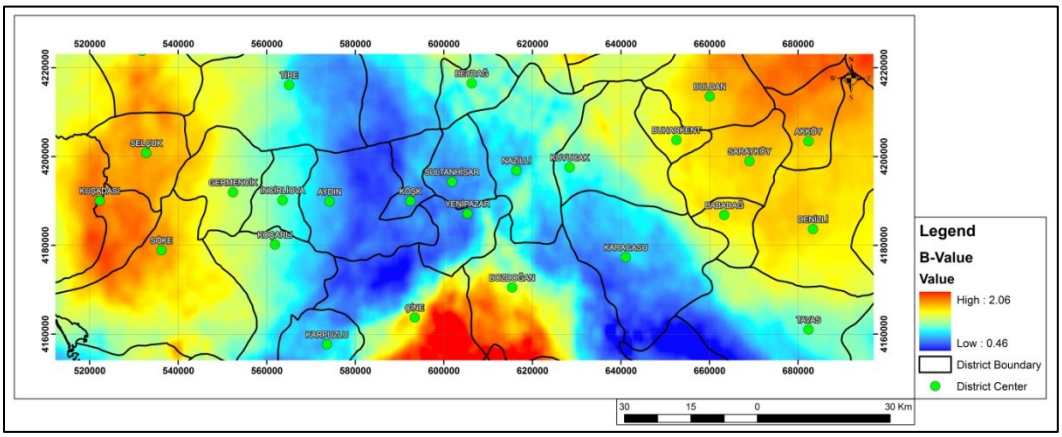


Figure 9. Gutenberg-Richter b-value map.

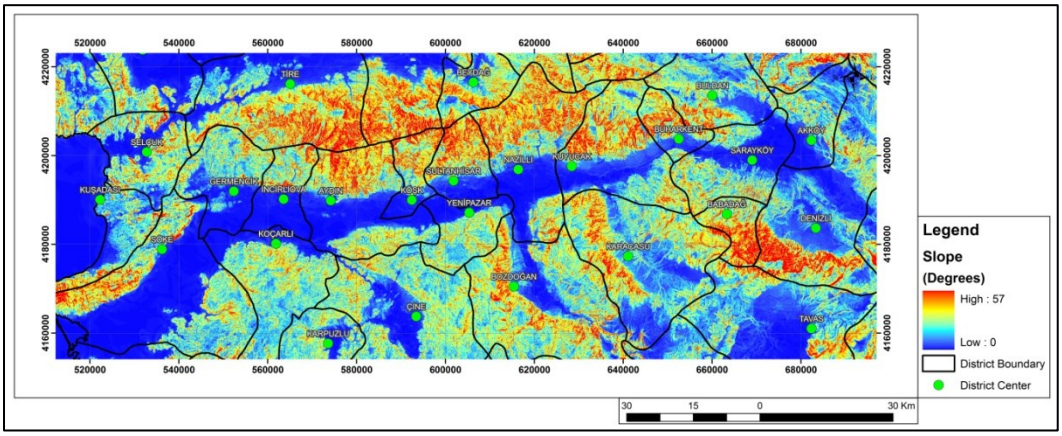


Figure 10. Slope map of the study area.

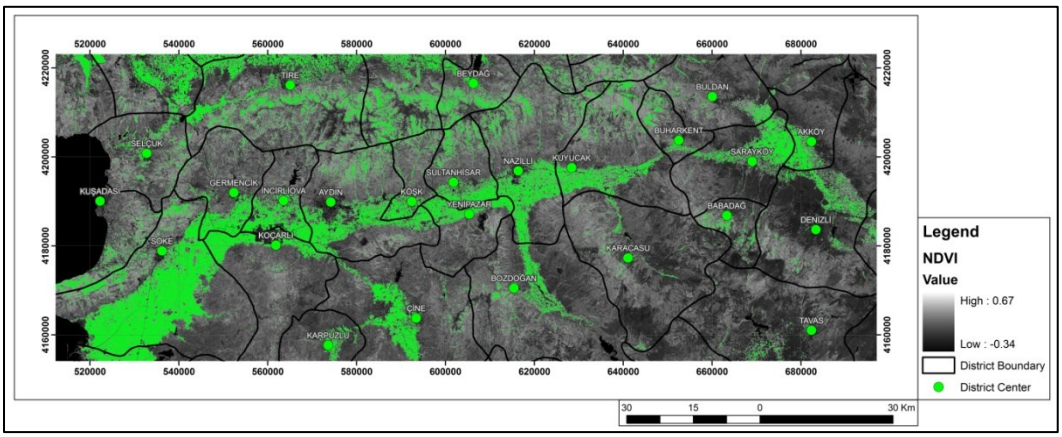


Figure 11. NDVI map with pixels above 0.353 threshold shown in green.

Finally each layer was weighted according to its relative importance in terms of its ability to reveal the geothermal potential (Table 2). Distance to fault and fault density were given the highest importance since the geothermal system under consideration is at an extensional regime where the flow is fracture controlled. Fault density particularly has the potential to reveal the highly fractured areas. Faulds (2010) pointed out that the intersections between normal faults and transversely oriented oblique-slip faults and overlapping oppositely dipping normal fault zones were observed in extensional geothermal fields. Fault density is included as a possible indicator of these regions. The total assigned weight to fault layer was divided among distance to fault and fault density. Thus, the fault density layer (60%) was given a slightly higher importance than distance to fault layer (40%) (Table 3). Hot springs are historically the major indicator of a geothermal system independent of the type of the system. Thus, in terms of relative importance, fault related layers were followed by the distance to the hot spring layer.

A geothermal system cannot exist in the absence of an overlaying cap rock to restrain the heat source. Therefore, the cap rock layer has been ranked third in terms of relative importance. Cap rock layer was followed by the distance to the graben layer. The

thickness of the main cap rock unit, being the Quaternary and Neogene units, decreases away from the graben center. This layer is not only included as an auxiliary to the distance to the cap rock layer but also to represent the asymmetric nature of the Büyük Menderes graben where most if not all geothermal activity is observed at the northern flank of the graben. The next layer in terms of relative importance is the night-time surface temperature layer, which is assigned a relatively low importance compared to previous layers due to its ability to only identify shallow systems as a temperature anomaly. The b-value layer is included as a seismo-tectonic parameter but is given a low importance since its correlation with geothermal favorability in extensional regimes is of debate. Tüfekçi et al., (2010) showed that about 75% of geothermal occurrence in the Western Anatolia region is correlated with higher b-values. However, Coolbaugh et al. (2003) argued that the relationship between high temperature geothermal systems and earthquake occurrences (earthquake moment release sum) is not correlated for extensional systems in the Great Basin, USA. Thus, the b-value layer is included but ranked low in the analysis. The b-value layer is followed by slope angle layer and NDVI layers which are indirect indicators of geothermal favorability. Slope angle layer accounts for the feasibility of geothermal development with regards to accessibility whereas the NDVI layer through highlighting the healthy vegetated areas indicates areas that are not suitable for geothermal development.

Table 2. Assigned criteria weights.

CRITERIA	RELATIVE IMPORTANCE	WEIGHT
Fault	1	0.36
Distance to Hot spring	2	0.23
Distance to Caprock	3	0.15
Distance to Graben Center	4	0.10
Night time Surface Temperature	5	0.07
Guttenberg - Richter b-value	6	0.04
Slope Angle	7	0.03
NDVI	8	0.02

Table 3. Assigned criteria weight for fault layer.

CRITERIA	WEIGHT
FAULT	0.36
Density (60%)	0.22
Distance (40%)	0.14

Finally TOPSIS methodology was applied on the weighted layers and the final favorability map was obtained. Final map is classified in 6 favorability classes according to equal area approach and the resultant map can be seen in Figure 12 and the number and percent of wells corresponding to each class are tabulated on Table 4. 213 of a total of 281 wells correspond to the class marked as most favorable, followed by 54 wells corresponding favorable and 11 wells corresponding to reasonably favorable classes. An insignificant number of wells (3) correspond to the remaining classes where no well correspond to the class marked as unfavorable.

Table 4. The number and percent of wells corresponding to each class.

CLASS	NUMBER OF WELLS	%	CATEGORY
6	213	75.80	Most favorable
5	54	19.21	Favorable
4	11	3.91	Reasonably favorable
3	2	0.71	Moderately favorable
2	1	0.36	Least favorable
1	0	0.00	Unfavorable

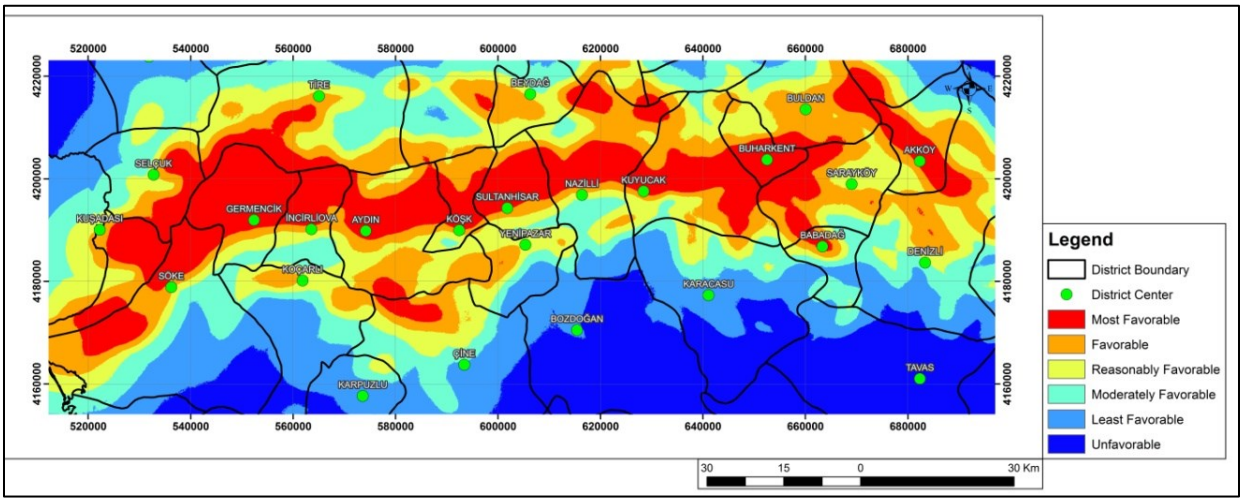


Figure 12. Geothermal Favorability Map.

4. CONCLUSIONS

In order to assess the geothermal favorability of Büyük Menderes Graben, a knowledge-based GIS-MCDA methodology has been followed. Analysis was performed on a total of nine standardized criteria maps, including distance to faults, fault density, distance to hot springs, distance to cap rocks, distance to the graben center, night time surface temperature, b-value, slope angle and NDVI. TOPSIS methodology, classified as an ideal point method, has been employed to obtain the final geothermal favorability map. Finally, the success of the favorability map was assessed by comparing the resultant map with the locations of the successful production wells in the area. As a result, 95% of the producing wells corresponded to the classes identified as most favorable (76%) and favorable (19%) followed by a 4% correspondence with reasonably favorable areas. The moderately favorable and least favorable classes were both below 1% and none of the producing wells corresponded to the class identified as unfavorable. 95% correspondence demonstrated that TOPSIS methodology applied in scope of this study is a useful tool to assess the geothermal favorability of Büyük Menderes graben. The criteria used in the analysis have been proven to be capable of revealing the true potential of the geothermal area under consideration. It should be noted that the particular set of data used in this study was only intended for extensional or amagmatic systems. Thus, they may fail to successfully identify favorable areas in a magmatic geothermal system. It is the intent of the authors of this study to meet its major purpose of guiding the search for new geothermal sources, hence leading to successful investments.

REFERENCES

Akkuş, İ., Akıllı, H., Ceyhan, S., Dilemre, A. and Tekin, Z.: Geothermal Resource Inventory of Turkey, MTA Genel Müdürlüğü Yayınları Envanter Serisi (In Turkish), 201, (2005).

Arslan, S., Akın, U., and Alaca, A.: Assessment of Crustal Structure of Turkey with Gravity Data, MTA Dergisi (In Turkish), 140, (2010), 57-73.

Bozkurt, E., & Sözbilir, H.: Evolution of the large-scale active Manisa Fault, Southwest Turkey: implications on fault development and regional tectonics, Geodinamica Acta, 19(6), (2006), 427-453.

Bozkurt, E., & Park, R. G.: Evolution of a Mid-Tertiary Extensional Shear Zone in the Southern Menderes Massif, Western Turkey, Bulletin de la Société Géologique de France, 168(1), (1997), 3-14.

Bozkurt, E.: Neotectonics of Turkey a Synthesis, Geodinamica acta, 14(1-3), (2001), 3-30.

Cambazoğlu, S., Yal, G.P., Eker, A.M., Şen, O. and Akgün, H.: Geothermal Resource Assessment of the Gediz Graben Utilizing TOPSIS Methodology, Geothermics, 80, (2019), 92- 102.

Coolbaugh, M.F., Sawatsky D.L., Oppliger G.L., Minor T.B., Raines G.L., Shevenell L.A., Blewitt G., Louie J.N.: Geothermal GIS Coverage of the Great Basin, USA: Defining Regional Controls and Favorable Exploration Terrains, Proceedings, Annual GRC Meeting, Morelia, Mexico, Oct. 12-15, Geothermal Resources Council Transactions, (2003).

Duman, T.Y., Emre, Ö., Doğan, A., Özalp, T., & Elmacı, H1: 250.000 Ölçekli Türkiye Diri Fay Haritası Serisi, Pafta No:NJ35-11, Maden Tetkik Arama (MTA), Ankara-Turkey, (2011).

Eneva, M., Coolbaugh, M.: Importance of Elevation and Temperature Inversions for the Interpretation of Thermal Infrared Satellite Images Used in Geothermal Exploration, Geothermal Resources Council Transactions, 33, (2009), 467–470.

Eyidoğan, H., Jackson, J.A.: A Seismological Study of Normal Faulting in the Demirci, Alasehir and Gediz Earthquake of 1969–1970 in Western Turkey: Implications for the Nature and Geometry of Deformation in the Continental Crust, Geophys. J. Royal Astron. Soc., 81, (1985), 569 - 607.

Faulds, J., Coolbaugh, M., Bouchot, V., Moek, I., Oguz, K.,: Characterizing Structural Controls of Geothermal Reservoirs in the Great Basin, USA, and Western Turkey: Developing Successful Exploration Strategies in Extended Terranes, Proceedings of World Geothermal Congress, France, (2010), 11 p.

Ferrill, D.A., J.A. Stamatakos, S.M. Jones, B. Rahe, H.L. Mckague, R.H. Martin, A.P.: Morris, Quaternary Slip History of the Bare Mountain Fault (Nevada) from the Morphology and Distribution of Alluvial Fan Deposits, Geology, 24, (1996), 559−562.

Gardner, J.K. and Knopoff, L.: Is the Sequence of Earthquakes in Southern California, with Aftershocks Removed, Poissonian Bulletin of the Seismological Society of America, 64, (1974),1363-1367.

General Command of Mapping:. 1:25,000 Scale Topographic Maps of Turkey, Ankara, (2000).

Gessner, K., Gallardo, L.A., Markwitz, V., Ring, U., Thomson, S.N.: What Caused the Denudation of the Menderes Massif: Review of Crustal Evolution, Lithosphere Structure, and Dynamic Topography in Southwest Turkey, Gondwana Res., 24, (2013), 243–274

Gutenberg, B., and Richter, C.F.: Seismicity of the Earth and Associated Phenomenon, Princeton University Press, Princeton, New York, (1949).

Görür N., Şengör A.M.C., Sakınç M., Tüysüz O., Akkök R., Yiğitbas¸ E., Oktay F.Y., Barka A.A., Sarıca N., Ecevitoğlu B., Demirbağ E., Ersoy Ş., Algan O., Güneysu C., Akyol A.: Rift Formation in the Gökova Region, Southwest Anatolia: Implications for the Opening of the Aegean Sea, Geol. Mag., 132, (1995), 637–650.

Gutiérrez, F.J., Lemus, M., Parada, M.A., Benavente, O.M., Aguilera, F.A.: Contribution of Ground Surface Altitude Difference to Thermal Anomaly Detection Using Satellite Images: Application to Volcanic/geothermal Complexes in the Andes of Central Chile, Journal of Volcanology and Geothermal Research, 237, (2012), 69-80.

Gürer, F. G., Sarıca-Filoreau, N.,Özburan, M.,Sangu, E., Doğan, B.: Progressive Development of the Büyük Menderes Graben Based on New Data, Western Turkey, Geol.Mag., (2009), 1-22.

Kahle, H.-G., M. Cocard, Y. Peter, A. Geiger, R. Reilinger, A.A. Barka, G. Veis,: GPS-derived Strain Rate Field within the Boundary Zones of the Eurasian, African, and Arabian Plates, J. Geophys. Res,. 105, (2000), 23353−23370.

Kiavarz, M., Jelokhani-Niaraki, M.,: Geothermal Prospectivity Mapping Using GIS-based Ordered Weighted Averaging Approach: A Case Study in Japan's Akita and Iwate Provinces, Geothermics, 70, (2017), 295-304.

Koçyiğit, A.: An Overview on the Main Stratigraphic and Structural Features of a Geothermal Area: The Case of Nazilli-Buharkent Section of the Büyük Menderes Graben, SW Turkey, Geodinamica Acta, 27:2-3, (2015), 85-109.

Koçyiğit A., Yusufoğlu H., Bozkurt E.: Evidence from the Gediz Graben for Episodic Two-stage Extension in western Turkey, J. Geol. Soc., London, 156, (1999), 605–616.

KOERI: Deprem Kataloğu (http://www.koeri.boun.edu.tr/sismo/2/earthquake-catalog/, date of access: 2019), (2019).

Malczewski, J.: GIS and Multicriteria Decision Analysis, John Wiley & Sons., (1999), 387 pp.

McKenzie, D.: Some Remarks on the Development of Sedimentary Basins, Earth Planet. Sci. Lett., 40, (1978), 25–32.

Menard, S.: Applied Logistic Regression Analysis, Sage University Series on Quantitative Applications in the Social Sciences, Thousand Oaks, CA: Sage, (1978).

MTA: 1/500.000 Scale Geological Maps, General Directorate of Mineral Research and Exploration (MTA), Turkey, (2002).

NASA LP DAAC, 2017. Aster Level 1 Precision Terrain Corrected Registered At-Sensor Radiance V003, NASA-EOSDIS,Land Processes DAAC. USGS Earth Resources Observation and Science (EROS) Center, Sioux Falls, South Dakota. https://doi.org /10.5067/Aster/Ast_L1t.003. Http://Earthexplorer.Usgs.Gov/, (Accessed on 15 January 2017). https://lpdaac.usgs.gov), (2017).

Noorollahi, Y., Itoi, R., Fujii, H., Tanaka, T.: GIS Model for Geothermal Resource Exploration in Akita and Iwate Prefectures, Northern Japan, Geothermics, 33, (2007), 1008-1021.

Noorollahi, Y., Itoi, R., Fujii, H., Tanaka, T.: GIS Integration Model for Geothermal Exploration and Well Siting, Geothermics, 37, (2008), 107–131.

Norusis, M.: SPSS 13.0 Guide to Data Analysis, Prentice Hall, Inc., Upper Saddle-River, NJ, (2004), pp. 13.

Richter, A.: Comparing Turkish Geothermal Development - with that in Indonesia - The Key Event of Turkey's Geothermal Energy Sector, Thinkgeoenergy, Webinar, Ankara , March, (2018).

Prol-Ledesma, R.: Evaluation of the Reconnaissance Results in Geothermal Exploration using GIS, Geothermics, 29 (1), (2000), 83–103.

Rogerson, P. A.: Statistical Methods for Geography, London: Sage, (2001).

Saaty, T.L.: The Analytic Hierarchy Process, McGraw-Hill, (1980), New York.

Seyitoğlu G. and Scott B.: Late Cenozoic Crustal Extension and Basin Formation in West Turkey, Geol. Mag., 128, (1991), 155–166.

Şengör A.M.C., Görür N., Şaroğlu F.: Strike-Slip Faulting and Related Basin Formation in Zones of Tectonic Escape: Turkey as a Case Study, In: Biddle K.T., Christie-Blick N. (Eds.), Strike-Slip Faulting and Basin Formation, Soc. Econ. Paleontol. Mineral. Sp. Pub., 37, (1985), 227–264.

Tüfekçi, N., Süzen, M.L., Güleç, N.: GIS Based Geothermal Potential Assessment: A case Study from Western Anatolia, Turkey, Energy, 35, (2010), 246-261.

USGS-EROS, Landsat 8 OLI/TIRS C1 Level 1 Archive, accessed online: http:// earthexplorer.usgs.gov, (Accessed on :15 January 2017).

Verge, N. J.: Oligo-Miocene Extensional Exhumation of the Menderes Massif, Western Anatolia, In Terra Abstracts, 7, (1995), p. 117.

Wiemer, S.: A Software Package to Analyze Seismicity: ZMAP, Seism. Res. Lett., 72, (2001), 373–382.

Yal, G., Eker A.M., Cambazoğlu, S., Şen, O. and Akgün, H.: Assessment of the Early Development Work for Kuyucak Geothermal Field, Turkey, 42nd Workshop on Geothermal Reservoir Engineering Stanford University, Stanford, California, February 13-15, (2017), SGP-TR-212.

Yalcin, M., Kilic Gul, F.: A GIS-Based Multi Criteria Decision Analysis Approach for Exploring Geothermal Resources: Akarcay Basin (Afyonkarahisar), Geothermics, 67, (2017), 18-28.

Yilmazer, S., S. Pasvanoglu, Vural, S.: The Relation of Geothermal Resources With Young Tectonics in the Gediz Graben (West Anatolia, Turkey) and Their Hydrogeochemical Analyses, Proceedings of World Geothermal Congress., (2010), 1-10.

Yousefi, H., Ehara, S., Noorollahi, Y.: Geothermal Potential Site Selection Using GIS in Iran, Proceedings, 32th Workshop on Geothermal Reservoir Engineering, Stanford University, Stanford University, (2007), 174–182.

Yousefi, H., Noorollahi, Y., Ehara, S., Itoi, R., Yousefi, A., Fujimitsu, Y., Nishijima, J.,Sasaki, K.: Developing the Geothermal Resources Map of Iran, Geothermics, 39, (2010),140–151.